ELSEVIER

Physics of the Earth and Planetary Interiors 118 (2000) 205–225

PHYSICS OF THE EARTH AND PLANETARY INTERIORS

www.elsevier.com/locate/pepi

The formation and evolution of layered structures in porous media: effects of porosity and mechanical dispersion

Stan Schoofs [a,*], Ron A. Trompert [a,1], Ulrich Hansen [b]

[a] *Vening Meinesz School of Geodynamics, Earth Science Institute, Utrecht University, Budapestlaan 4, 3584 CD, Utrecht, Netherlands*
[b] *Institut für Geophysik, Westfälische Wilhelms-Universität Münster, Corrensstraße 24, D-48149, Münster, Germany*

Received 8 October 1998; received in revised form 8 October 1999; accepted 20 October 1999

Abstract

Horizontally layered structures can develop in porous or partially molten environments, such as hydrothermal systems, magmatic intrusions and the early Earth's mantle. The porosity ϕ of these natural environments is typically small. Since dissolved chemical elements unlike heat cannot diffuse through the solid rocks, heat and solute influence the interstitial fluid density in a different manner: heat advects slower than solute through the liquid by the factor ϕ, while diffusion of heat through the bulk porous medium is larger by the factor ϕ^{-1} times the ratio between the thermal and chemical diffusivities. By performing numerical experiments in which a rigid low-porosity medium is heated from below, we have studied the formation and evolution of layers in an initially stably stratified liquid. Growth of a convective layer through convective entrainment, the formation of a stable density interface on top of the layer and destabilization of the next layer are intimately linked. By monitoring the heat (solute) fluxes, it is observed that the transport of heat (solute) across the interface changes from convective entrainment towards a regime in which transfer is purely diffusive (dispersive). Because this transition occurs before the stage at which the lower layer arrives at the thermal equilibrium, we conclude that the layer growth stops when the density interface on top has grown sufficiently strong to keep the ascending plumes in the lower layer from convectively entraining more fluid from above. A simple balance between the most important forces, exerted on a fluid parcel in the lower layer, is proposed to determine this transition. This force balance also indicates whether a density interface keeps intact, migrates upwards or breaks down during the further evolution of the layered sequence. Finally, mechanical dispersion tends to increase transport of chemically dissolved elements across the density interface. Since this reduces the density difference between the two adjacent layers, the thickness of the lower layer increases.

Keywords: Layering; Thermochemical convection; Hydrothermal systems; Magma

1. Introduction

Layering is a characteristic geological feature on nearly every scale. These horizontally layered structures can develop in porous or partially molten systems, such as magmatic intrusions (Cawthorn, 1996), hydrothermal systems (Griffiths, 1981; Bischoff and

* Corresponding author. Tel.: +31-30-253-5142; fax: +31-30-253-5030; e-mail: schoofs@geo.uu.nl

[1] Now at Origin Nederland, Bakenmonde 2, 3434 KK, Nieuwegein, Netherlands.

0031-9201/00/$ - see front matter
PII: S0031-9201(99)00148-X

Rosenbauer, 1989; Fournier, 1990; Williams, 1997; Lowell and Germanovich, 1997), or the early Earth's mantle (Stevenson, 1989; Olson et al., 1990). We are therefore interested in the generation and evolution of layers within the fluid, which percolates through the pores and fractures of the solid rocks. In magmatic systems, growth of crystals by reaction with the interstitial liquid can subsequently lead to the solidification of chemically distinct layers like those observed in outcrops of magma chambers. The development of vertically stacked convective layers in hydrothermal systems, however, reduces the vertical transport of heat and chemical elements as compared with single-layered flow (Griffiths, 1981) and has, therefore, implications for the crustal evolution. As a first-order approximation, the magmatic and hydrothermal systems can be represented by a rigid porous medium (Phillips, 1991; Aharonov et al., 1997), of which the porosity ϕ is typically smaller than 10 vol.%

It has been shown that under several circumstances thermochemical convection of purely viscous fluids is a vital mechanism to produce layering (Turner, 1968; McBirney and Noyes, 1979; Spera et al., 1986; Hansen and Yuen, 1995; Alley and Parmentier, 1998). Thermochemical convection is a fluid dynamical phenomenon, where two substances with different diffusivities (heat and compositional concentration of dissolved elements) are the sources of buoyancy (Turner, 1985).

In the context of flow in porous media, thermochemical convection has been treated both analytically and experimentally in previous studies and was reviewed by Nield and Bejan (1992). Generally, the convection takes the form of a boundary layer flow (Murray and Chen, 1989). Laboratory experiments in porous media showed that a thin density interface between two convective layers can be maintained against diffusive thickening (Griffiths, 1981). This is essential for the persistence of individual convecting layers.

When a fluid moves through a porous medium, heat and chemical elements are transported by (1) diffusion through the solid framework, (2) diffusion through the interstitial liquid and (3) advection of the liquid. Although diffusion of heat through the solid and liquid is of the same order, diffusion of chemical components is generally much larger through the liquid than through the solid. Therefore, heat and dissolved elements influence the interstitial fluid density in a different manner. Temperature perturbations advect more slowly than salinity fluctuations by the factor ϕ, but diffuse more rapidly by the factor κ/D and so are smoothed out more efficiently. Here, ϕ is porosity, while κ and D denote the thermal and chemical molecular diffusivity, respectively. This leads to the development of double-advective, double-diffusive instabilities (Phillips, 1991), especially in cases where porosity is small.

We consider the case where destabilization of the fluid is accomplished by imposing a positive temperature contrast at the bottom, while the compositional concentration is initially stably stratified. In hydrothermal systems, for example, this resembles the situation in which hot magma approaches an initially chemically stably stratified pore fluid from below.

In a previous study on layer formation in porous systems, in which the porosity was chosen equal to a hypothetical value of $\phi = 1$, thermochemical convection was shown to be a good potential candidate to generate layered structures (Schoofs et al., 1998). In this so-called Hele–Shaw approximation, however, heat and solute advect at the same speed, which is fundamentally different from flow through a geological medium having a low porosity. A single experiment with a porosity of $\phi = 0.1$ showed that, although the gross features of the layer formation resemble those observed in Hele–Shaw experiments, there exist a number of significant differences between the flow within these two media (Schoofs et al., 1998).

In this study, we have performed numerical experiments in the more realistic setting of a low-porosity medium. Despite the significant numerical challenge we have decided to do so to be able to investigate the potential role of thermochemical convection as a layer forming mechanism in a natural porous medium. Comparing these results with those, as obtained in Hele–Shaw cells, enables us to delineate specific features of double-diffusive, double-advective flow as present in convection in low-porosity environments.

Beyond the interest in the evolution of geological systems, the experiments will shed some light on fundamental differences in the fluid dynamics of convection in porous media and in purely viscous

flow (in the following free flow, in contrast to flow in porous media). Since inertial forces do not exist in porous media flow, significant differences are to be expected. For example, entrainment of nonbuoyant fluid from a density gradient into a convective region is reduced by the absence of inertial forces. Further, drag forces exerted by the solid rock dominate over viscous coupling. Due to the lack of advection or diffusion of vorticity in porous media flow, the flow geometry is different from that of free flow. Moreover, viscous dissipation of energy is proportional to the square of velocity but it does not depend on the actual flow geometry (Shen and Veronis, 1991). This is also different from energy dissipation in free flow, which is mainly caused by viscous coupling between the fluid parcels (Batchelor, 1967). Viscous coupling involves the spatial derivatives of velocity and, therefore, it is related to the scale of convection. Understanding these fluid dynamical phenomena is of vital interest towards a better understanding of the dynamics of the envisaged geological systems.

In addition to advective and diffusive transport of chemical elements, hydrodynamic mixing of the interstitial fluid at the pore scale also leads to chemical transfer. This type of mixing, called mechanical dispersion, is due to obstructions and the fact that all pores may not be accessible to a fluid element after it has entered a particular flow path (Nield and Bejan, 1992). Due to substantial heat diffusion through the solid rocks, mechanical dispersion of heat in the liquid is negligible under most geological circumstances. A further set of experiments addresses the chemical dispersion explicitly.

The outline of the paper is as follows. In Section 2, the governing equations describing flow in a porous medium and the employed numerical method are given. The results of two sets of experiments with first, a simple and, next, a velocity-dependent dispersion model are discussed in Section 3. After a concise description of the major features of the layer formation, we focus on the differences in fluid dynamical behavior observed in low-porosity media and Hele–Shaw cells. Attention is paid to the variation in the vertical scales of the convective layers. Finally, the sensitivity of the layer-forming mechanism to the most important parameters is discussed. We conclude the paper by summarizing the results, and discussing the geological implications of this work.

2. Formulation

We have considered a two-dimensional homogeneous porous medium in a rectangular domain of aspect ratio A, which is saturated with fluid (see Fig. 1a). The horizontal and vertical Cartesian coordinates are denoted by x and z, respectively. In real-

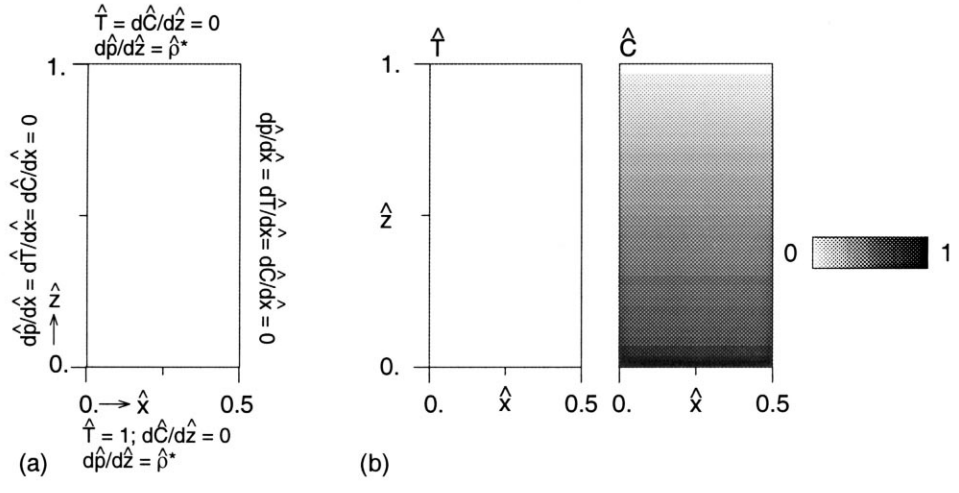

Fig. 1. (a) Geometrical setup and boundary conditions of the experiment in the porous medium and (b) initial conditions.

ity, the flow is evidently three dimensional (Murray and Chen, 1989). However, the essential physics involving layer formation in a two-dimensional model are, at least in free flow, similar to those in three dimensions (Molemaker and Dijkstra, 1997). Furthermore, these authors pointed out that a high-resolution numerical study was required to resolve the very thin density interfaces. Therefore we feel that a high-resolution study in two dimensions fits our purposes better than a three-dimensional one on a rather coarse grid.

Conservation of mass of an incompressible fluid in a porous medium is described by (Nield and Bejan, 1992)

$$\nabla \cdot \boldsymbol{q} = 0, \tag{1}$$

where $\boldsymbol{q}$ is the seepage velocity.

Assuming that inertia effects are negligible, conservation of momentum in the porous medium is expressed by Darcy's law

$$\boldsymbol{q} = -\frac{K}{\mu}(\nabla p - \rho \boldsymbol{g}), \tag{2}$$

with p for pressure, ρ for density, and $\boldsymbol{g}$ for the gravitation vector. The permeability K is assumed to be isotropic and spatially invariant, while the dynamic fluid viscosity μ is taken as a constant.

Conservation of energy can be expressed as

$$\sigma\frac{\partial T}{\partial t} - \kappa\nabla^2 T + \boldsymbol{q} \cdot \nabla T = 0, \tag{3}$$

where it is assumed that the fluid and matrix are in thermal equilibrium and the effective thermal diffusivity of the saturated medium κ is constant. T is the temperature, subscript t is the time derivative, and σ represents the ratio of the heat capacities between the solid matrix and the fluid $\sigma = \phi + (1-\phi)(\rho c_p)_{\text{matrix}}/(\rho c_p)_{\text{fluid}}$. Here c_p represents the heat capacity and ϕ is the porosity. Finally, note that mechanical dispersion of heat is neglected.

When we assume that the dispersive flux of compositional concentration can be expressed in Fickian form (Bear, 1972), conservation of the solute concentration C is described as:

$$\phi\frac{\partial C}{\partial t} - \nabla \cdot (\mathbf{D}_h \nabla C) + \boldsymbol{q} \cdot \nabla C = 0, \tag{4}$$

where $\mathbf{D}_h$ is a second-order tensor describing the hydrodynamic dispersion.

Two Fickian models of solute dispersion are considered. In the first and most simple model, the hydrodynamic dispersion term is represented by a constant scalar, D_{eff}, multiplied by porosity:

$$\phi\frac{\partial C}{\partial t} - \phi D_{\text{eff}}\nabla^2 C + \boldsymbol{q} \cdot \nabla C = 0. \tag{5}$$

In the second model a more refined treatment of dispersion is considered, which is often used in groundwater flow studies (Bear, 1972). The hydrodynamic dispersion tensor, $\mathbf{D}_h$, is now given by the sum of the molecular diffusion in the porous medium, $\mathbf{D}_{\text{mol}}$, and the tensor of mechanical dispersion $\mathbf{D}_{\text{mech}}$. Here, the molecular diffusion in the porous medium is defined as $\mathbf{D}_{\text{mol}} = \phi\mathbf{D}_f/\tau$, where $\mathbf{D}_f$ is the molecular diffusivity of the chemical component within the fluid and τ the tortuosity of the porous medium. The coefficients of $\mathbf{D}_{\text{mech}}$ are a function of both fluid velocity and medium characteristics. In general, mechanical dispersion of chemical concentration is much larger than $\mathbf{D}_{\text{mol}}$, except when the flow is very slow. For this second dispersion model, the conservation of species is expressed as:

$$\phi\frac{\partial C}{\partial t} - \nabla \cdot \left([\mathbf{D}_{\text{mol}} + \mathbf{D}_{\text{mech}}]\nabla C\right) + \boldsymbol{q} \cdot \nabla C = 0, \tag{6}$$

where $\mathbf{D}_{\text{mech}}$, written in scalar terms, is given by

$$(\mathbf{D}_{\text{mech}})_{ij} = (a_l - a_t)\frac{q_x q_z}{|\boldsymbol{q}|} + a_t|\boldsymbol{q}|\delta_{ij}. \tag{7}$$

Here, a_l and a_t represent the longitudinal and transversal dispersivities, respectively. Furthermore, δ_{ij} is the Kronecker delta. For a nonlinear treatment of mechanical dispersion, the reader is referred to the work of Hassanizadeh and Leijnse (1995).

The laws for conservation of mass, momentum, energy, and species and a linearized equation of state $\rho = \rho_0[1 - \alpha(T - T_0) + \beta(C - C_0))$ (reference values are denoted by the subscript 0) describe thermochemically driven flow in porous media mathematically. Here α and β are the coefficients of thermal and chemical expansion, respectively. The equations are nondimensionalized with the height of the domain h as the length scale, $h^2\sigma/\kappa$ as timescale, $\mu\kappa/K$ as characteristic pressure scale, and $\Delta T = T - T_0$ and $\Delta C = C - C_0$ as the temperature and

chemical scale, respectively. This results in the following set of differential equations

$$\hat{\nabla}^2\hat{p} = Ra_T\left(R_\rho\frac{\partial\hat{C}}{\partial\hat{z}} - \frac{\partial\hat{T}}{\partial\hat{z}}\right) = \frac{\partial\hat{\rho}^*}{\partial\hat{z}} \tag{8}$$

$$\frac{\partial\hat{T}}{\partial\hat{t}} - \hat{\nabla}^2\hat{T} + \hat{\boldsymbol{q}}\cdot\hat{\nabla}\hat{T} = 0, \tag{9}$$

and for the species equation, in case of the scalar dispersion model

$$\phi^*\frac{\partial C}{\partial t} - \hat{\nabla}\cdot\left(\frac{1}{Le_{\text{eff}}}\hat{\nabla}\hat{C}\right) + \hat{\boldsymbol{q}}\cdot\hat{\nabla}\hat{C} = 0, \tag{10}$$

where the circumflexes denote the nondimensionality of a parameter, while $\hat{\rho}^* = \hat{\rho} - \hat{\rho}_0 = Ra_T(R_\rho\hat{C} - \hat{T})$ is the difference between the density and the density at the reference state.The four dimensionless parameters governing the convective dynamics are the thermal Rayleigh number Ra_T, the buoyancy ratio R_ρ, ϕ^*, and an effective Lewis number, Le_{eff}.These dimensionless parameters are defined as

$$Ra_T = \frac{\alpha K_0\,\rho g\Delta Th}{\kappa\mu}, \quad R_\rho = \frac{\beta\Delta C}{\alpha\Delta T},$$

$$\phi^* = \phi/\sigma, \quad Le_{\text{eff}} = \frac{\kappa}{D_{\text{eff}}}.$$

The heat capacity ratio is chosen equal to $\sigma = 1$ in this study, a reasonable assumption for most natural systems. As a result, the parameter ϕ^* is smaller than one in flow of (nearly) incompatible elements in low-porosity systems. Comparison of Eq. (9) with (10) shows that these chemical elements are advected at the fluid velocity $\boldsymbol{q}/\phi^*$, while heat advects with the total fluid flux $\boldsymbol{q}$. This leads to the development of double-advective, double-diffusive instabilities (Phillips, 1991).

In case of the more complete dispersion model, Eq. (10) is replaced by:

$$\begin{aligned}\phi^*\hat{C}_{\hat{t}} + \hat{q}_x\frac{\partial\hat{C}}{\partial x} + \hat{q}_z\frac{\partial\hat{C}}{\partial z} &= \frac{\partial}{\partial\hat{x}}\left(\left(f1 + \frac{1}{Le_{\text{mol}}}\right)\frac{\partial\hat{C}}{\partial\hat{x}} + f3\frac{\partial\hat{C}}{\partial\hat{z}}\right)\\ &\quad + \frac{\partial}{\partial\hat{z}}\left(f3\frac{\partial\hat{C}}{\partial\hat{x}} + \left(f2 + \frac{1}{Le_{\text{mol}}}\right)\frac{\partial\hat{C}}{\partial\hat{z}}\right),\end{aligned} \tag{11}$$

where

$$f1 = \frac{\hat{a}_{\text{t}}\left(a_{\text{r}}\hat{q}_x^2 + \hat{q}_z^2\right)}{|\hat{\boldsymbol{q}}|} \quad f2 = \frac{\hat{a}_{\text{t}}\left(a_{\text{r}}\hat{q}_z^2 + \hat{q}_x^2\right)}{|\hat{\boldsymbol{q}}|}$$

$$f3 = \frac{\hat{a}_{\text{t}}\left((a_{\text{r}} - 1)\,\hat{q}_x\hat{q}_z\right)}{|\hat{\boldsymbol{q}}|} \quad a_{\text{r}} = a_{\text{l}}/a_{\text{t}}$$

$$Le_{\text{mol}} = \frac{\kappa}{\mathbf{D}_{\text{mol}}}.$$

In this study, the model is set up in a rectangular domain with impermeable and free-slip boundaries (see Fig. 1a). A thermal contrast is imposed at the bottom, while the temperature at the top is fixed to zero. The vertical walls are insulators with respect to heat transport, while all sides satisfy no-flux conditions for the solute. Initially, the motionless interior is cold and the solute concentration is stably stratified, having a linear gradient $\partial\hat{C}/\partial\hat{z} = 1$ (Fig. 1b). In dimensionless form, the boundary and initial conditions are defined as:

$$\hat{x} = 0,\ A\colon \partial\hat{p}/\partial\hat{x} = \partial\hat{T}/\partial\hat{x} = \partial\hat{C}/\partial\hat{x} = 0,$$

$$\hat{z} = 0\colon \partial\hat{p}/\partial\hat{z} = \hat{\rho}^*;\ \hat{T} = 1;\ \partial\hat{C}/\partial\hat{z} = 0,$$

$$\hat{z} = 1\colon \partial\hat{p}/\partial\hat{z} = \hat{\rho}^*;\ \hat{T} = 0;\ \partial\hat{C}/\partial\hat{z} = 0,$$

$$\hat{t} = 0\colon \hat{T} = 0;\ \partial\hat{C}/\partial\hat{z} = 1.$$

In the following, the circumflexes denoting the nondimensionality of the parameters are omitted.

The system of equations is solved on a cell-centered grid by using a second-order finite volume multigrid method. Details of the method are given by Trompert and Hansen (1996), where it was used for free convection at infinite Prandtl number. Spatially, a central approximation is used for the diffusive fluxes. Furthermore, the flux-limited Fromm scheme (Sweby, 1984; Hundsdorfer and Trompert, 1994) is used for the advective compositional fluxes to preserve the monotonicity of the solution at sharp interfaces. The nonlimited version of this scheme is used for the advective thermal fluxes.

Time integration is carried out by an implicit Crank–Nicolson method for the diffusion of heat and for the chemical dispersion in the simple scalar model. The second-order explicit Adams–Bashforth scheme is used to advance the velocity-dependent chemical dispersion terms in time. This Adams–Bashforth scheme is also employed for the advective

terms. Validation of the code was accomplished by comparison with published results on thermo(chemical) convection in porous media (Kimura et al., 1986; Rosenberg and Spera, 1992; Oldenburg and Pruess, 1995).

3. Results

The main objective of this study is to understand the formation and evolution of vertically stacked convective layers in low-porosity systems. Therefore a number of calculations has been carried out with various values of Ra_T, R_ρ, ϕ^*, and a_1, in a domain with aspect ratio $A = 0.5$. The numerical discretization used is 128×256 cells, based on extensive testing of the accuracy of the solutions by using various grids and varying time step size.

First, the observations on the generation of convective layers in a typical low-porosity experiment are described. The parameters are $Ra_T = 5 \times 10^4$, $R_\rho = 4$, and $\phi^* = 0.1$. An effective chemical dispersion coefficient is taken, which is 100 times lower than the thermal diffusivity ($Le_{\text{eff}} = 100$). Next, the results of this experiment are compared with those observed in a Hele–Shaw cell in which $\phi^* = 1$. In Section 3.2, the data are analyzed to understand what limits the height of the growing convective layers. The variety of the layer scales is discussed in terms of a balance between the most important forces acting on a fluid parcel in the lower layer (Section 3.3). A sensitivity study of the layer generating mechanism as a function of the most important parameters is presented in Section 3.4. In the final section (Section 3.5) the influence of mechanical dispersion of chemical on the layer formation is discussed.

3.1. Layer formation

In Fig. 2, the thermal, compositional and absolute velocity distributions are shown at four different stages in the evolution. A dark shading indicates a high value, while a light shading means a low temperature, a depleted compositional concentration or a low velocity. Fig. 3a–c displays the corresponding vertical profiles of horizontally averaged temperature, composition and density. In Fig. 3d, a set of different density profiles are displayed to provide an overview of the evolution of the layer formation.

Fig. 2a and profiles i in Fig. 3 display a thin thermal boundary layer developing at the bottom. Due to the large temperature difference across this layer, it becomes unstable almost instantaneously. Several convective plumes rise from this boundary layer into the cold and compositionally lighter environment. The region near the bottom is rapidly mixed by the rising and sinking currents, leading to a chemically almost uniform layer with increasing temperature. The ascending plumes erode the initial density gradient by incorporating the nonbuoyant fluid into the convective layer. This mechanism, which we call ''convective entrainment'', increases the layer thickness with time.

Between the plume heads and the overlying (motionless) fluid a sharp, stable density interface develops. The stability of the density jump arises from the difference in solute content between the convective layer and the motionless fluid above the interface. The vast majority of the plumes are stopped by this interface, while only the most vigorous ones are able to entrain further some material from the upper layer. While low solute flux across the interface keeps the interface intact, heat flux destabilizes the overlying fluid. As a result, a small convective layer develops on top of the lower one (see Fig. 2b and profiles ii in Fig. 3). This second layer also grows vertically by entraining fluid from above.

Convective mixing in the upper layer increases the chemical difference between the two layers, while the diffusive heat flux across the interface reduces the temperature difference across the interface. Both processes lead to a further increase of the density difference $\Delta\rho_{\text{int}}$ between both layers. As a result, fewer and fewer plumes can entrain material from above such leading to a further decrease in the growth rate. Fig. 2c and profiles iii in Fig. 3 show the stage, in which the growth rate of the first layer is virtually zero. Advective mixing of the fluid in the second layer results in a chemically uniform layer with sharp boundary layers. The fluid on top of the second layer has also become unstable, which indicates that a third layer will soon be generated. All together, a staircase of well-mixed convective layers develops, which are separated by sharp diffusive/

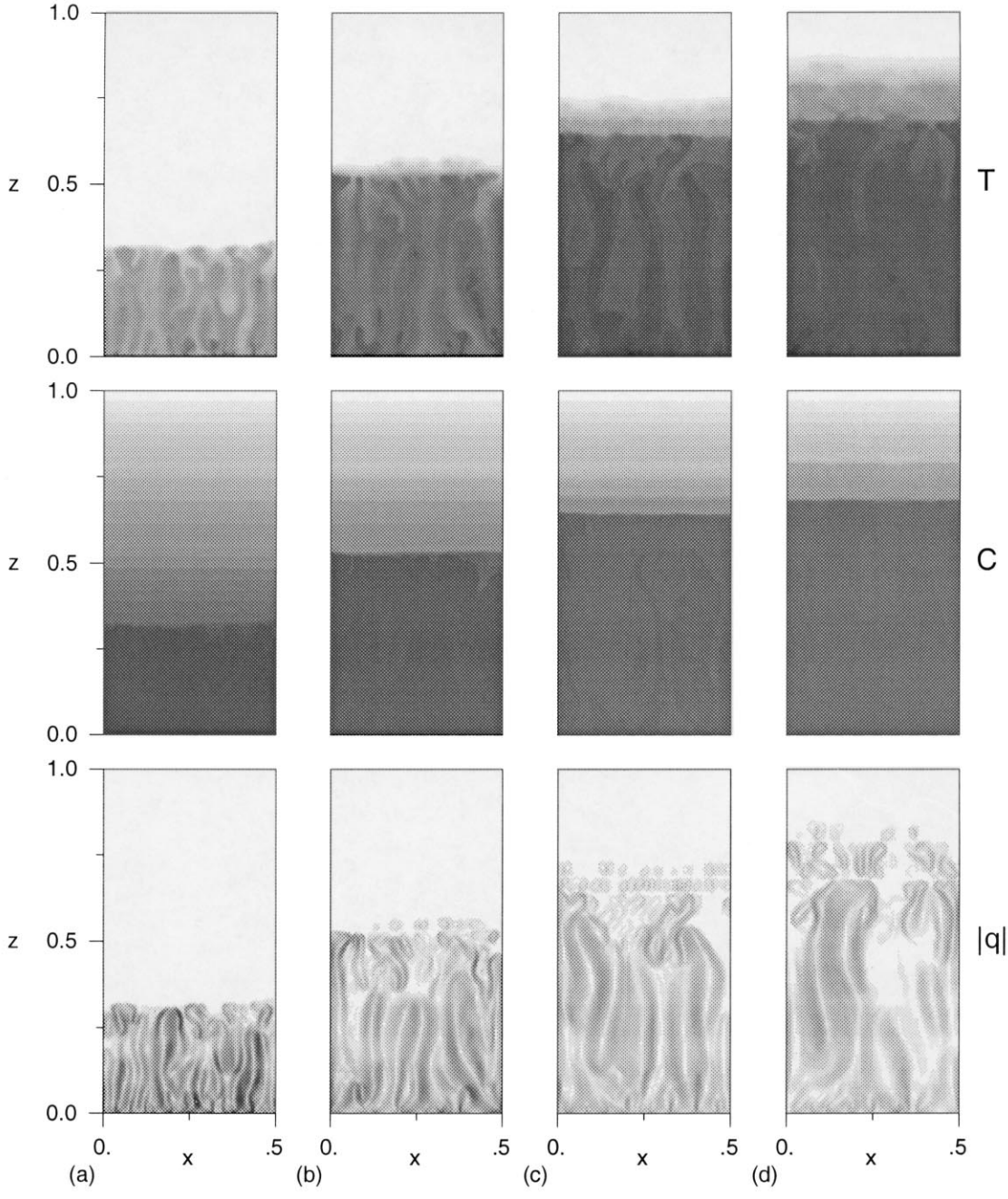

Fig. 2. Snapshots of temperature T, compositional concentration C, and absolute velocity $|\mathbf{q}|$ of a simulation with $Ra_T = 5 \times 10^5$, $R_\rho = 4$, $Le_{\text{eff}} = 100$, and $\phi^* = 0.1$ at (a) $t = 0.000438$, (b) $t = 0.002788$, (c) $t = 0.004733$, and (d) $t = 0.007951$. Dark (light) shading indicates high (low) temperature or enriched (depleted) compositional concentration. Dimensionless T and C scale is between 0 and 1, while velocity scale ranges from 0 to 8500.

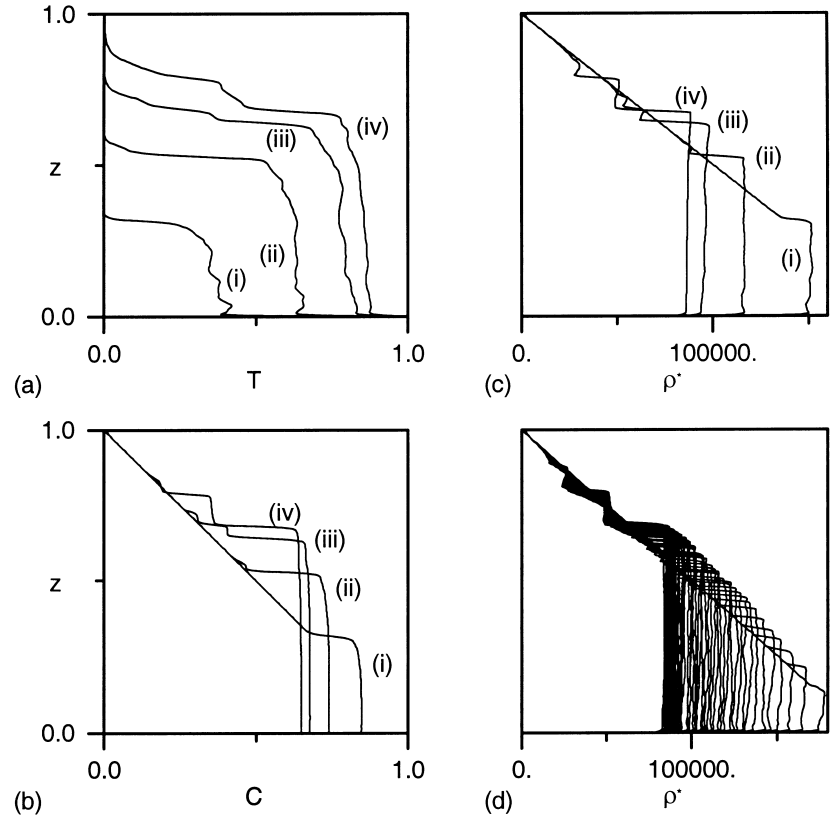

Fig. 3. Transient development of horizontally averaged profiles at the same times as in Fig. 2. (a) Temperature T. (b) Compositional concentration C. (c) Density $\rho^* = \rho - \rho_0 = Ra_T(R_\rho C - T)$. (d) Same as (c), but at many more times between $t = 0.0$ and $t = 0.01$. The development and sharpening of several interfaces is clearly shown.

dispersive interfaces. Note that the lowermost layer is much thicker than the other ones.

Fig. 2d and profiles iv in Fig. 3 depict the situation at a later stage, in which the second and third layers have merged again and the amalgamated layer has just reached its maximal thickness. Note that another layer initiates on top of the amalgamated layer. When the heat that enters the domain through the bottom is sufficiently large to destabilize all fluid, the convective layers will reach the top of the domain and the interfaces start to break down one after each other from the top down (not shown). Ultimately, one chemically homogeneous convective layer remains.

Up to now, the gross features of the layer formation in a low-porosity medium resemble those observed in experiments in a Hele–Shaw cell (in which $\phi^* = 1$). For a more detailed description of the layer formation, the reader is referred to Schoofs et al. (1998). There exist, however, a number of significant differences in the evolution of the convective layers within these two media. To reveal these differences a simulation with $\phi^* = 1$ has been performed, while keeping the other parameters as before.

Fig. 4 depicts snapshots of the T and C fields and the horizontally averaged profiles of T, C and ρ^*, at the same stage as Fig. 2b and the profiles ii in Fig. 3. Two layers have developed in the lower part of the domain, while a third one just destabilizes. Furthermore, the density contrast across the interface between the first two layers is relatively small (the profile of ρ^* shows that $\Delta\rho^*_{\mathrm{int}} \approx 5 \times 10^3$). Hence, the interface fluctuates considerably.

The most striking difference is that, at the stage shown, the first convective layer in the low-porosity experiment has already grown significantly larger

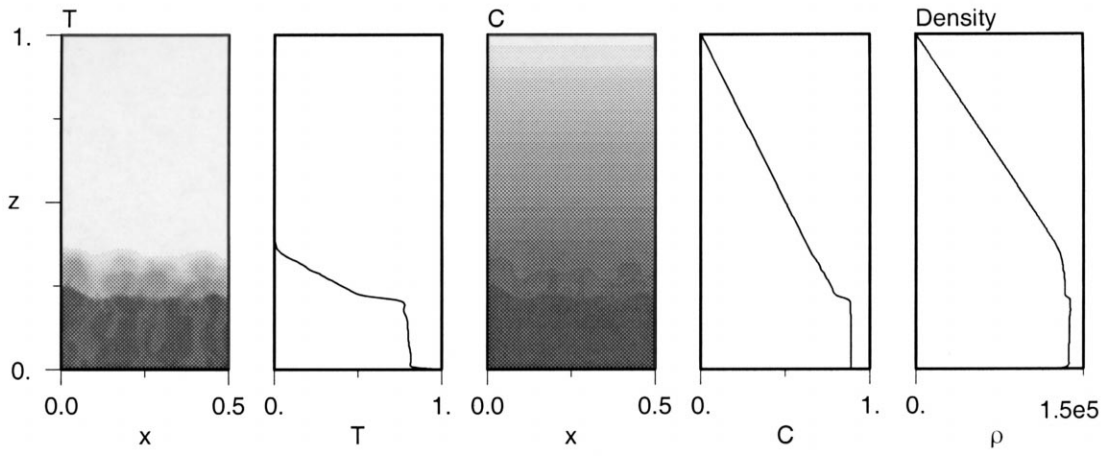

Fig. 4. Snapshots of the T and C fields and the horizontally averaged profiles of T, C and ρ of a Hele–Shaw experiment, plotted at the same stage as the snapshots (b) and profiles (ii) of the previous figures. Parameters are $Ra_T = 5 \times 10^5$, $R_\rho = 4$, $Le_{\text{eff}} = 100$, and $\phi^* = 1$.

($h = 0.52$), as compared with the first layer in the Hele–Shaw experiment ($h = 0.21$). The average temperature of the first layer, however, is lower in the low-porosity medium. Due to the high advection rate of the solute in a low-porosity medium, virtually all available potential energy is instantaneously converted into kinetic energy. Heat that enters the domain through the bottom therefore leads to advective homogenization of the chemical field (and thus fast layer growth), rather than to an increase of internal energy of the convective layer (by advecting heat upwards).

A consequence of the relatively fast layer growth in the low-porosity medium is that the density jump on top of the layer also grows at a faster rate, than is the case in the Hele–Shaw experiment (compare the density profiles). This phenomenon will turn out to be of significant importance for the self-limiting mechanism of the convective layers. Due to the fast growth of the density contrast between the convective layer and the motionless fluid, the interface is virtually flat almost from the point of destabilization of the convective layer.

Another specific feature of low-porosity flow is that fluid exchange occurs on small lateral scales, compared with Hele–Shaw flow. We attribute this feature to the difference in advective speeds of heat and solute again. At lower porosities, enhanced advective but reduced diffusive transfer of chemical concentration results in a flow geometry in which smaller lateral scales are preferred. Due to the lack of viscous coupling particular to flow in porous media (Shen and Veronis, 1991), the slender flow pattern does not inherently lead to an extreme loss of energy by viscous dissipation, as would be the case for free flow. The rapid exchange of chemically buoyant (depleted) and relatively heavy (enriched) fluid is, at least locally, a very efficient mixing mechanism.

Finally, we note that the ascending plumes often detach from the bottom thermal boundary layer in the low-porosity experiments, rather than ascending straight to the top of the convective layer (as is the case in Hele–Shaw experiments). The ascending plume parts deflect or split when encountering sinking currents.

3.2. Self-limitation of the convective layers

Of vital importance in understanding the layer formation is the question of what limits the convective layer to a certain height. In Hele–Shaw experiments, two mechanisms become operative nearly at the same stage during the evolution of the first layer (Schoofs et al., 1998). First, transport of heat (solute) across the interface changes from convective entrainment towards pure diffusion (dispersion) across the interface. In this mechanism, the density jump on top of the layer has grown sufficiently large to prohibit

the plumes from entraining fluid from above into the convective layer. Note that this mechanism determines the limitation of the layer growth in free flow (Fernando, 1987; Molemaker and Dijkstra, 1997).

The second mechanism limiting the layer growth in Hele–Shaw cells is, that the convective layer reaches a thermal equilibrium. At this equilibrium, the heat flux through the horizontal boundary layers of the convective layer are equal, while the average temperature of the layer is constant. Consequently, the layer has stopped growing and the flow within resembles a statistically steady state. The flow does not really reach a statistically steady state, because diffusive (dispersive) interfacial heat (solute) transfer erodes the density jump across the interface on a compositionally dispersive timescale. This mechanism of arrival at a thermal equilibrium was actually proposed as to determine the limitation of the convective layers in Hele–Shaw cells (Schoofs et al., 1998).

A third mechanism was proposed earlier for free flow and it implies that a stationary situation is reached when entrainment from below the interface by convection in the upper layer balances entrainment from above the interface by convection in the lower layer (Turner, 1968; Huppert and Linden, 1979). Though this mechanism has been shown to be unimportant for the Hele–Shaw case (Schoofs et al., 1998), it might be a possible cause of the layer limitation in low-porosity flow.

To investigate if and which one of these mechanisms is relevant in low-porosity media, we have focused our attention on the evolution of the first convective layer. The different stages can be summarized as follows (Fig. 5): in the first phase the layer grows very fast by entraining fluid from above the interface (from the start up to arrow 2). Meanwhile, a density jump develops on top of the convective layer. This is followed by a period of decreased growth rate (stage confined between arrows 2 and 3). During this phase, the density difference across the interface on top of the first layer grows further gradually. Moreover, the fluid above the interface becomes unstable, leading to the formation of the second layer. After this intermediate stage, finally, another sharp decrease in the growth rate is observed (arrow 3). From this point, the thickness of the first layer increases only very slowly up to the end of the simulation. Arrow 4 corresponds with the stage at which the second layer stops growing. This is discussed in Section 3.3.

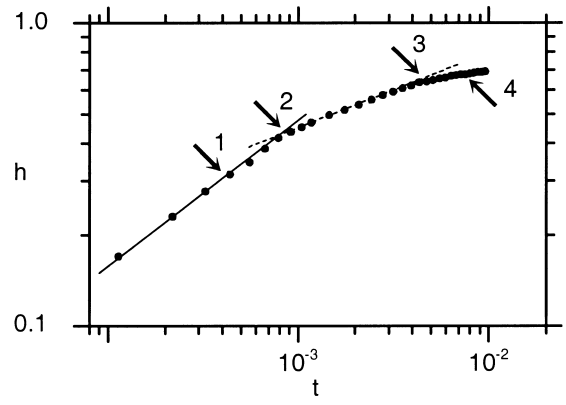

Fig. 5. Temporal evolution of the height h of the first layer of the low-porosity experiment depicted in Figs. 2 and 3. The numbered arrows indicate the times of the snapshots and profiles depicted in the previous figures.

To distinguish between the three mechanisms, we have monitored the transport properties near the interface. For the balanced entrainment mechanism to be relevant, one expects a significant advective component of heat and mass flux across the interface. The two other mechanisms, on the contrary, are characterized by a transition from convective towards purely diffusive/dispersive interfacial transport. In dimensionless form, the horizontally averaged diffusive (dispersive) flux of heat (solute) is given by

$$-\frac{\overline{\partial T}}{\partial z}; \quad -\frac{\overline{\partial C}}{\partial z} \tag{12}$$

and the advective flux by

$$\overline{wT}; \quad \frac{Le_{\mathrm{eff}}}{\phi^*}\overline{wC}. \tag{13}$$

The results of the measurements are shown in Fig. 6. Horizontally averaged fluxes are plotted at four time instants, corresponding to those marked in Fig. 5 (the dashed profiles of the fourth instant and will be discussed in Section 3.3). Each profile has been time averaged over a number of profiles around these time instants. As expected, in the well-mixed

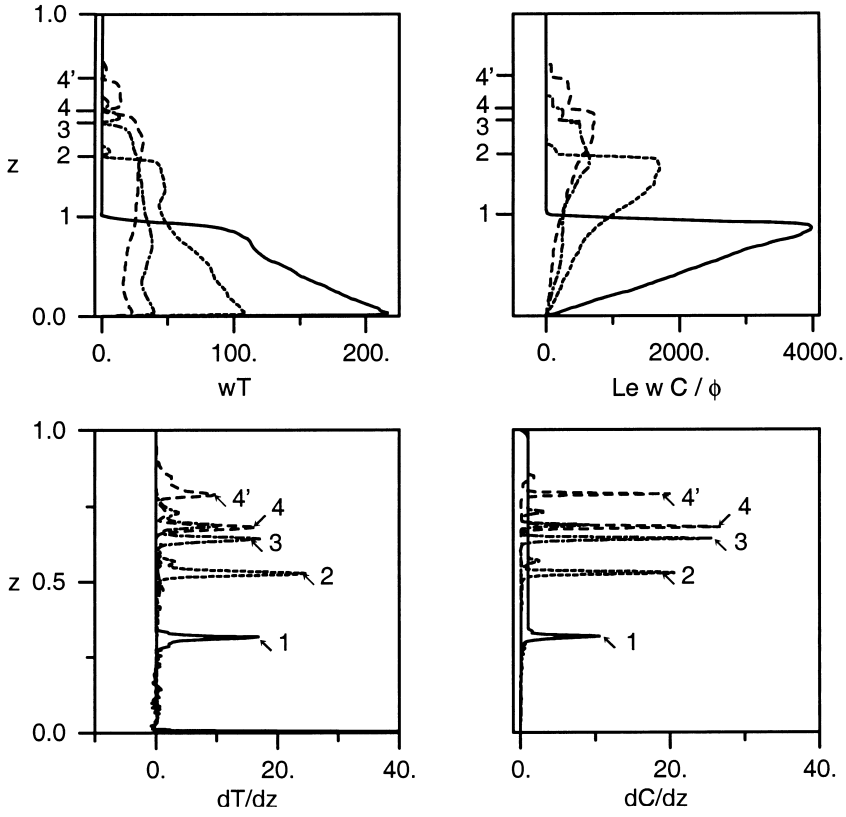

Fig. 6. Horizontally averaged diffusive/dispersive and advective fluxes of T and C, as defined in (12) and (13), plotted as a function of depth at the same four stages in the evolution as in the previous figures. (a) $t = 0.000438$ (solid curves), (b) $t = 0.002788$ (dotted), (c) $t = 0.004733$ (dash-dotted), and (d) $t = 0.007951$ (dashed). The numbers indicate the position of the first interface in the diffusive/dispersive profiles. Number 4′ indicates the second interface at the fourth stage.

convecting layer the advective fluxes are much larger than the diffusive ones. Moreover, the magnitude of the compositional advective flux is much larger than that of heat again, due to both a high Le_{eff} and a low porosity.

At the first time instant (solid curves), the advective components of both heat and solute fluxes dominate the transport on top of the convective layer. This indicates that fluid is advectively entrained from above into the first layer. The sharp peaks in the diffusive profiles demonstrate the flatness of the interface (at $z = 0.31$, indicated by arrow 1).

At the second time instant (dotted curves), the advective component of the heat flux across the interface is approximately zero, while the advective solute flux still dominates the dispersive one. Entrainment across the interface has decreased, because the density difference between the two convective layers has increased. Nevertheless, fluid from the second layer is entrained slowly into the lowermost one.

Finally, the dash-dotted curves show the fluxes shortly after the second change in the growth rate. The position of the interface is at $z = 0.64$, denoted by arrow 3. At this stage, both heat and solute fluxes across the interface are diffusively/dispersively dominated.

The flux measurements across the interface thus reveal a transition from a regime in which convective entrainment dominates, towards a regime in which the transport is purely diffusive/dispersive. These findings, therefore, rule out the mechanism of balanced entrainment and seem to indicate that either the transition in the entrainment regime itself, or the

arrival at a thermal equilibrium, limits the convective layers. It is remarkable to say that these observations resemble closely the observations in Hele–Shaw cells.

One way to distinguish between these two remaining mechanisms is by comparing the total flux of the driving component (heat) through the horizontal boundary layers of the lowermost layer. For the first mechanism to be valid, the heat flux through the interface is still smaller than the bottom heat flux, at the stage when the layer growth stops. A necessary condition for the second mechanism to be valid is, that these two fluxes are equal at this stage.

The heat fluxes through both boundary layers of the first convective layer are compared at the same three time instants as before. Heat flux through the bottom of this layer is always purely diffusive, because the bottom of the domain is impermeable. At the position just above the bottom boundary layer, the advective heat flux is nearly equal to the bottom heat flux. At the first time instant, the bottom heat flux is equal to 142 dimensionless units, which is much larger than the total heat flux through the sharp density interface. During the stage of decreased growth rate, the bottom heat flux is approximately 74 dimensionless units, three times larger compared to the interfacial heat flux. At the moment when the layer growth stops, the bottom heat flux is approximately 41, still more than twice as large compared to the heat flux across the interface (which is equal to 17).

From these measurements, we can conclude that the layer growth stops before the first layer arrives at the thermal equilibrium. We therefore favor the transition in the entrainment regime, as to determine the final thickness of this layer in low-porosity systems. When the density jump on top of the layer becomes sufficiently strong to prohibit the plumes to entrain fluid from above, heat (solute) transfer across this interface becomes purely diffusive (dispersive). Note that this mechanism is different from the one which limits the layer growth in Hele–Shaw cells (Schoofs et al., 1998). Despite the lack of inertial and viscous forces, however, the limiting mechanism in porous media flow is similar to that in free flow (Molemaker and Dijkstra, 1997). Further heating of the layer leads only to minimal additional growth until the thermal equilibrium is reached.

The next question we want to answer is, what determines the transition in heat and solute transport across the interface. In free flow, this transition in the entrainment regime is described by a balance between the kinetic energy of the lower convective layer and the potential energy across the interface (Fernando, 1987; Molemaker and Dijkstra, 1997).

At first glance, a similar balance could also determine the transition in transport mechanism in porous media flow. For the buoyancy-driven convection of a fluid in a porous material, however, inertia is negligible (see Section 2). In other words, the flow reacts instantaneously on the buoyancy and pressure gradients present in the fluid. Rather than an energy balance, a balance between the buoyancy forces acting on the fluid just beneath the interface seems therefore to be more appropriate to describe the transition in low-porosity flow.

In Fig. 7, a schematic diagram of the convecting bottom layer is shown, the density interface and the convecting layer on top of the interface. A fluid parcel just beneath the interface experiences the following forces. First, the upward convective force $\mathbf{F}_{\mathrm{conv},1}$ is given by the buoyancy of the parcel minus the pressure gradient, divided by ϕ^*:

$$\mathbf{F}_{\mathrm{conv},1} = \frac{\overline{\rho^* - p_z}}{\phi^*} = \frac{w}{\phi^*}, \tag{14}$$

where Darcy's law has been used. Subscript 1 denotes that it is the convective force, which is present in the first layer. The factor ϕ^* is included because the solute advects upwards with a speed of w/ϕ^*, rather than w. Obviously, the vertical velocity be-

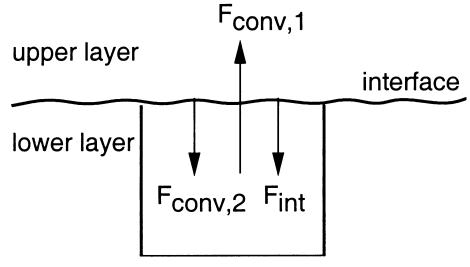

Fig. 7. Schematic diagram of two convective layers separated by a density interface. A fluid parcel just beneath the interface experiences two forces: a convective force of the lower layer $\mathbf{F}_{\mathrm{conv},1}$, and a buoyancy force due to the density difference across the interface $\mathbf{F}_{\mathrm{int}}$.

comes negligible at the interface, which would give a convective force $\mathbf{F}_{\mathrm{conv},1}$ equal to zero. This can be seen in Fig. 8a, in which the vertical profiles of both the horizontally averaged and maximum vertical velocity are plotted, just at the stage at which the layer growth stops. As an alternative, a representative value of the upward velocity in the lower layer can be taken as to represent the convective force. Since only the most vigorous plumes are able to scrape off the interface, we choose the maximal vertical velocity $w_{\max}$ in the lower convective layer, divided by ϕ^*, as the convective force $\mathbf{F}_{\mathrm{conv},1}$.

The second force, which acts on the fluid parcel, is exerted by the stable density interface and is directed downwards. Its dimensionless, absolute value is given by $|\mathbf{F}_{int}| = |\overline{\Delta\rho^*_{int}}|$, which is the horizontally averaged density difference across the interface. A third force, the downward convective force $\mathbf{F}_{\mathrm{conv},2}$ in the upper layer is neglected here, because it is still small at the moment when the layer growth stops.

We suggest that the transition in the entrainment regime occurs when:

$$\mathbf{F}_{\mathrm{conv},1} = c_1|\mathbf{F}_{\mathrm{int}}|, \tag{15}$$

where c_1 should be of order $O(1)$. To check this force balance, we have plotted both forces as a function of time (Fig. 8b). The downward interfacial force $|\mathbf{F}_{\mathrm{int}}|$ initially increases strongly with time towards a value of 2.70×10^4 at $t \approx 0.0001$. From this point, $|\mathbf{F}_{\mathrm{int}}|$ grows at a significantly lower rate. The convective force $\mathbf{F}_{\mathrm{conv},1}$, however, first decreases strongly. At a later stage, the force decreases further gradually until an almost statistically steady value is reached. At the moment when the layer growth stops ($t \approx 0.0045$), $\mathbf{F}_{\mathrm{conv},1} \approx 3.60 \times 10^4$ and $|\mathbf{F}_{\mathrm{int}}| \approx 3.92 \times 10^4$, which means that a constant c_1 of order $O(1)$ is obtained. This is a clear indication for the proposed force balance to be appropriate.

3.3. Variation in layer thicknesses

A typical feature of the layer formation is that the first convective layer is much thicker than all of the others that are fairly similar in scale (see Fig. 2c,d). This might indicate that the final height of these next layers is determined by another mechanism, than is the case for the first layer.

To gain insight in the evolution of these other layers, we have examined the evolution of the amalgamated second layer. From the fluxes (Fig. 6, dashed curves), we have observed a transition from convective entrainment towards pure diffusion (dispersion) of heat (solute) across the interface on top of this layer (indicated by arrow 4′). Moreover, the growth of this layer is limited before a thermal equilibrium has been reached. This can be seen in Fig. 6 by

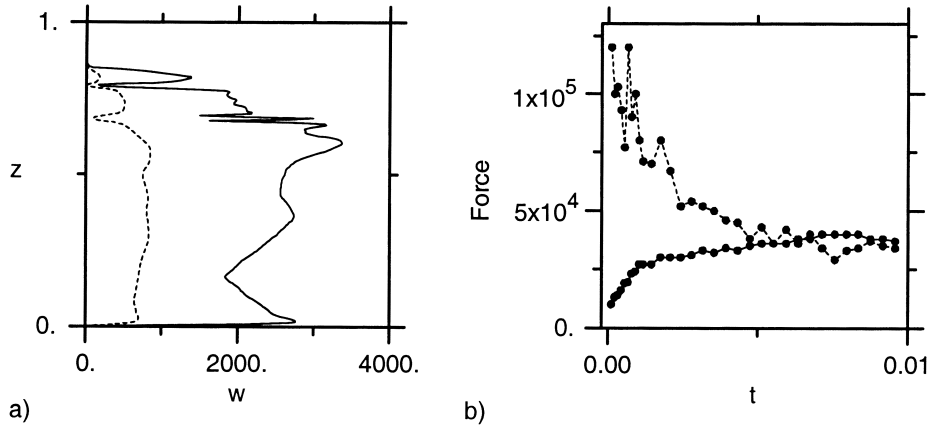

Fig. 8. (a) Vertical profiles of the lateral maximum of the vertical velocity $w_{\max}$ (solid curves), and of the horizontally averaged vertical velocity (dotted), at the moment when the layer growth stops ($t = 0.004733$). (b) The two forces depicted in Fig. 7, $\mathbf{F}_{\mathrm{conv}}$ (solid) and $|\mathbf{F}_{\mathrm{int}}|$ (dotted), plotted as a function of time.

comparing the diffusive heat fluxes near arrows 4 and 4′ (as the advective heat fluxes are equal to zero across these interfaces). Since the mechanism, which limits this second layer, is similar to the mechanism that determines the layer height of the first layer, something else must be responsible for the difference in layer scales.

In our view, the temporal evolution of the vertical velocity, and thus the convective force, explains why the first layer is so much larger than all of the others (see Fig. 8b). Just after destabilization of the bottom thermal boundary layer, the thermal contrast between the rising plumes and the still cold interior is huge. Consequently, the vertical velocities of these plumes, and thus the convective forces, are also very large. The increase of the temperature in the convective layer with time leads to a gradual decrease of the plume velocities, until from $t \approx 0.005$ the maximal velocity is statistically constant. The interfacial density force, however, increases almost linearly with the thickness of the convective layer, but does not depend on the particular stage of the evolution. The force balance for the second layer is therefore reached already at a lower layer depth, as compared with the one for the first layer.

The gradual decrease of velocity in time towards a statistically constant value thus explains both the relatively larger thickness of the first layer and the almost equal vertical scales of the subsequent layers.

There are two kinds of events that influence the structure, on a timescale much shorter compared to the dispersive one. These are gradual upward ''migration'' and sudden ''breakdown'' of the interface. Both phenomena are described in detail for the Hele–Shaw experiments by Schoofs et al. (1998), but have also been observed in the present study at low porosity. These phenomena become better understandable in the frame of the proposed force balance.

For upward ''migration'' of an interface to occur, two conditions must be met. First, the convective force in the lower layer must be stronger than in the upper one. Secondly, the interfacial density force must be equal or smaller than the convective force in the lower layer. The rising plumes in the lower layer can then entrain fluid across the interface.

The ''breakdown'' of an interface occurs, however, when the convective forces in the two layers adjacent to the interface are equal to each other and, further, also approximately equal to the density force. In this setting, the convection currents in both layers deflect the interface. When the amplitude of the deflections becomes so large that the interface touches the interface above, the interface breaks down.

3.4. Parameter dependence

In this section, the sensitivity of behavior of the layer-forming mechanism to the most important parameters is described. In the first set of experiments the thermal Rayleigh number has been varied, while the other parameters are fixed to $R_\rho = 3$ and $\phi^* = 0.1$. For Rayleigh numbers up to $Ra_T < 15 \times 10^3$, the heat flux through the bottom is not large enough to destabilize more than one layer. At larger Ra_T, several layers are generated in the way as described in Section 3.1, where the number of layers that form increases with increasing Ra_T. Fig. 9a shows the final thickness of the first layer h_f as a function of Ra_T, for five simulations in this multiple layer regime. The results indicate that a power law relation exists between h_f and Ra_T, with an exponent of 0.2.

Since a higher Ra_T leads to a higher vertical velocity in the lowermost layer and thus to a larger convective force, this relatively low exponent seems unexpectedly low. From the experiments, we suggest the following relation between Ra_T and the maximum vertical velocity w_{max}:

$$w_{max} \propto Ra_T^{1.0}. \quad (16)$$

Therefore, the low sensitivity of the layer thickness on Ra_T must imply that besides the vertical velocity, the density difference across the interface also increases strongly with increasing Ra_T. This is understandable, because R_ρ is kept constant. Apparently, the forces associated with these two quantities increase at an almost similar rate.

Next, four experiments have been performed in which R_ρ is varied, while $Ra_T = 5 \times 10^4$ and $\phi^* = 0.1$. Fig. 9b shows the resulting inverse relationship between the final layer thickness h_f and the buoyancy ratio R_ρ:

$$h_f = 0.9 R_\rho^{-1.4}. \quad (17)$$

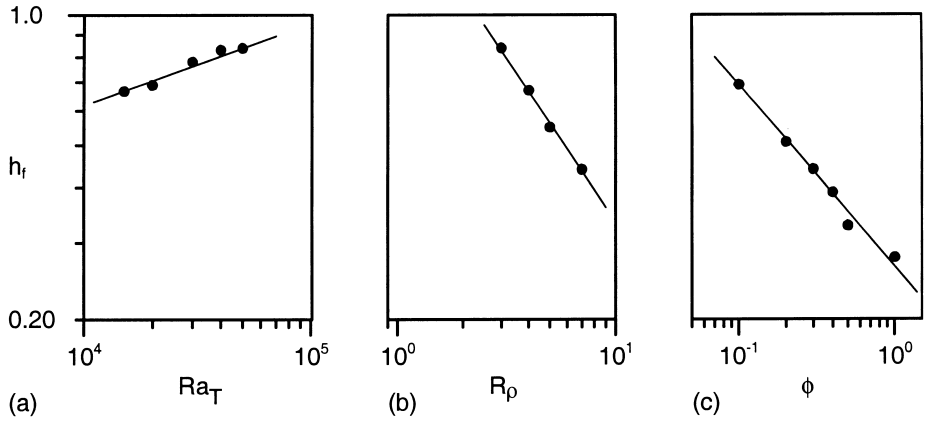

Fig. 9. Sensitivity of behavior of the layer formation as a function of the most important parameters. (a) The final layer height of the first layer h_f as a function of Ra_T for a constant buoyancy ratio $R_\rho = 3$ and $\phi^* = 0.1$. (b) The final layer height h_f, but now as a function of R_ρ, while the Rayleigh number is fixed to $Ra_T = 5 \times 10^4$, and porosity is kept at $\phi^* = 0.1$. (c) The final thickness of the first layer h_f, but now as a function of ϕ^*, while $Ra_T = 5 \times 10^4$ and $R_\rho = 3$.

Assuming that convection has been well developed in a layer, the interior of the layer is compositionally uniform. This means that the chemical field only influences the boundary layers. Consequently, the vertical velocity and thus the convective force of the first layer is merely a function of Ra_T (see (16)), and depends only weakly on the buoyancy ratio R_ρ. A higher chemical buoyancy, however, enhances the growth of the density contrast across the interface such explaining the large negative exponent in (17).

In a further set of experiments porosity is varied, which is motivated by the fact that porosity is typically very small in magmatic and hydrothermal systems ($\phi \approx O(10^{-4}$ to $10^{-1})$). Flow at the very low porosities can not be resolved numerically in this study. For flow in media with a porosity of $\phi = 0.01$, the reader is referred to Schoofs et al. (1999). To find the relation between porosity and the final layer thickness h_f, we have performed six simulations in which porosity ranges from 1 to 0.1 (Fig. 9c). The other parameters are fixed at $Ra_T = 2 \times 10^4$, $^{R}_{\rho} = 3$ and $Le_{eff} = 100$. A simple power law, which describes the data, is

$$h_f = 0.28\phi^{*-0.4}. \quad (18)$$

This relationship shows, that porosity does not only influence the convective force $\mathbf{F}_{conv}$ within the lower layer (since in that case $h_f \propto \phi^{*-1}$, see (14), but also leads to a faster growth of the interfacial density force F_{int}.

3.5. Mechanical dispersion

In the previous experiments, we have assumed an effective chemical dispersion coefficient, which is 100 times lower than the effective thermal diffusivity of the saturated medium. For the large velocities observed during the layer formation, however, mechanical dispersion may play a significant role in the transport of chemical elements. Laboratory experiments (Griffiths, 1981) showed that mechanical dispersion indeed modifies the chemical flux across a stable density interface between two convecting layers considerably. The scalar model (10) employed in the previous experiments is not very accurate in handling mechanical dispersion of chemical elements and is therefore be replaced by the more advanced tensor model (11) (Bear, 1972).

At present, both the longitudinal dispersivity a_l and the dispersivity ratio a_r that appear in (11) are poorly known in geological media (Gelhar et al., 1992). In crustal domains of less than a hundred meters, laboratory, borehole and field tests seem to indicate that the longitudinal dispersivity is related to the scale of the flow domain systematically. However, the longitudinal dispersivity flattens to a value

of around 1–10 m for a domain scale of around 100 m, suggesting that this so-called ''scale-effect'' does not proceed to regional scales. The transversal dispersivity follows this behavior, but at values that are smaller by an order of magnitude. In partially molten magmatic systems, these hydraulic parameters are also not known very well. The layer-forming mechanism studied here may be applicable to either of these geological systems, which differ both in length scale and structure of the solid framework. The amount of mechanical dispersion can therefore vary significantly among these systems, justifying a sensitivity study of the layer formation to dispersion of chemical elements.

We have performed six experiments in which the longitudinal dispersivity has been varied between two extreme values ($a_l = 10^{-2}$ and 10^{-5}) while the dispersivity ratio is kept at $a_r = 10$. The molecular diffusivity of the chemical component is taken 10^4 times smaller than the effective thermal diffusivity ($Le_{mol} = 10^4$). Other parameters are $Ra_T = 10^5$, $R_\rho = 3$, and $\phi^* = 0.5$.

Fig. 10 depicts snapshots of the temperature and chemical fields of two experiments, at the same stage in the evolution. For a case in which the dispersivity is low ($a_l = 10^{-5}$, Fig. 10a), the final thickness of the first convective layer has just been reached.The observed layer height is nearly similar to that of the lowermost layer generated in the simple scalar dispersion experiment (in which $h_f = 0.48$, see Fig. 9c). Furthermore, several layers have developed on top of each other in a manner that resembles the mechanism observed in the experiments with a simple scalar dispersion model fairly well.

In a system in which the longitudinal dispersivity is equal to 10^{-3} times the depth of the system, however, the dimensionless height of the first layer is already significantly larger at the same stage in the evolution (Fig. 10b). Longitudinal dispersion of chemical elements in the ascending plumes and in less extent also transversal dispersion in currents along the interface mix the chemical content of the first layer with that of the fluid above the interface. Since these processes reduce the density difference across the interface, the plumes in the lower layer can entrain more fluid from above. This results both in a faster growth rate and a larger final thickness of the first layer, as compared with the low-dispersion experiment shown in Fig. 10a. Finally, an even larger longitudinal dispersivity ($a_l = 10^{-2}$) enables the first layer to grow to the top of the domain and prevents the generation of any other layers. In Fig.

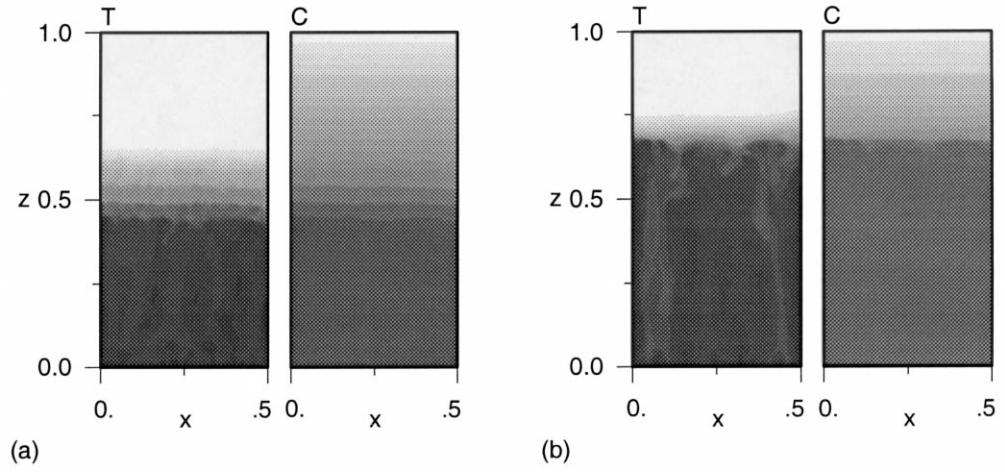

Fig. 10. Snapshots of temperature and compositional concentration of two experiments at a similar stage during the evolution ($t = 0.0046$). The longitudinal dispersivity is (a) $a_l = 10^{-5}$ and (b) $a_l = 10^{-3}$. Other parameters are: $Ra_T = 10^5$, $R_\rho = 3$, $\phi^* = 0.5$, $Le_{mol} = 10^4$, and $a_r = 10$.

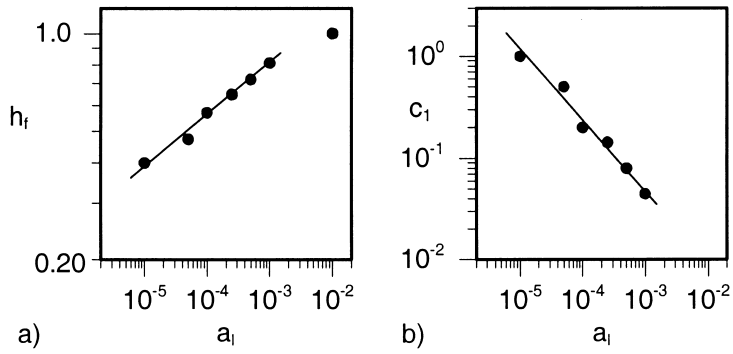

Fig. 11. Sensitivity of behavior of the layer formation as a function the longitudinal dispersivity a_l. Other parameters are $Ra_T = 10^5$, $R_\rho = 3$, $\phi^* = 0.5$, $Le_{mol} = 10^4$, and $a_r = 10$. (a) The final layer height of the first layer h_f, and (b) the value that c_1 must take to fit the force balance (15).

11a, the final thickness of the first layer h_f is plotted for the six experiments as a function of a_l.

Mechanical dispersion of chemical elements clearly increases the amount of entrainment across the interface. Therefore, it must be taken into account in the force balance (15), which determines the transition in the entrainment regime. Since the convective layer for $a_l = 10^{-2}$ is limited by the vertical extent of the domain, this data point has not been considered here. Fig. 11b depicts the value that the constant c_1 in (15) should take to match the two forces at the moment when the layer growth stops, as a function of a_l. When we assume that transversal dispersion is negligible, a more complete force balance of the form

$$\mathbf{F}_{conv,1} = 10^{-5} a_l^{-0.7} |\mathbf{F}_{int}|. \quad (19)$$

is derived.

4. Discussion and conclusions

In this study, the formation and evolution of horizontally layered structures has been investigated in a rigid medium of low porosity. To do so, a temperature contrast was imposed at the bottom of a compositionally stably stratified interstitial liquid. In the first set of numerical experiments, chemical dispersion is represented by a simple effective scalar model. The results from these experiments show that thermochemical convection is a vital mechanism for the generation of layered structures in media with a geologically realistic porosity.

The gross features of the layer formation resemble those observed in Hele–Shaw cells. A convective layer develops at the bottom of the domain, which grows by incorporating fluid from above. Since this layer is convectively mixed, a stable density jump develops on top of the layer. The fluid overlying this density interface is destabilized by considerable heat flux across the interface, while low solute flux keeps the interface intact. In this way a staircase of well-mixed convective layers develops, of which the lowermost layer is much thicker than all of the others. The layers are separated by sharp diffusive/dispersive interfaces.

We have shown that the limitation of the first layer to a certain depth is not a consequence of destabilization of the next layer, as was proposed earlier for free flow (Turner, 1968). In our configuration, the layer growth is limited by the formation of a sufficiently strong density interface on top of the layer. Consequently, the transport of heat (solute) across the interface changes from convective entrainment towards pure diffusion (dispersion). In that sense our results differ from those on flow in Hele–Shaw cells, where the layer growth is limited due to the arrival at the thermal equilibrium (Schoofs et al., 1998).

We attribute the difference in the limiting mechanisms to fundamental differences in the fluid-dynamical behavior in these two media. In low-porosity

media heat advects slower than solute by the factor of porosity, while in Hele–Shaw cells both quantities advect at the same speed. As a result, thermal energy that enters the low-porosity domain through the bottom is converted into kinetic energy, rather than increasing the internal energy of the convective layer. Advective homogenization of the chemical field results in a relatively fast growth of the density interface on the top of the first layer. Consequently, the transition in the entrainment regime has occurred before the layer arrives at the thermal equilibrium. Note that despite the lack of inertia and viscous coupling, the limiting mechanism is similar to the one observed in free flow (Fernando, 1987; Molemaker and Dijkstra, 1997).

A simple balance between the most important forces exerted on a fluid parcel in the lower layer is proposed as to determine the limitation of the layer growth. The layer growth stops when the upward convective force of the lower layer becomes smaller than the downward directed force exerted by the stable density difference across the interface. The depth of the layer is determined by the amount of fluid that can be entrained within the period before the transition in the entrainment regime has occurred.

The next step in determining the actual time scale involved with the formation of the layers is to extend the force balance concept to a reduced model of the layer growth of the form $\partial h/\partial t = f(Ra_T, R_\rho, \phi^*, h)$ (see also Molemaker and Dijkstra (1997) for a reduced model for free flow). However, setting up such a reduced problem needs a more precise parameterization of the heat flux across the interface and of the convective forces within the layer(s). Therefore, setting up the reduced model goes beyond the scope of this study.

The variation of layer thickness between the first and other layers is ascribed to a decay of the convective forces in time, towards a statistically steady value. Since these other layers develop at a later stage in the evolution of the system, the convective forces in these layers are lower compared to the force that enabled the first layer to grow. As a result, the transition in the entrainment regime takes already place at smaller layer thicknesses.

Once it is established, an interface can vanish through several mechanisms. Besides the ultimate disappearance of any interface through diffusional/dispersive homogenization, our experiments have shown that on short timescales (1) the migration of an interface and (2) the breakdown of an interface can lead to sudden changes of the layer structure. These intermittent changes determine the vertical scales of the convective layers, rather than the initial layer growth. The different behavior of these two dynamical mechanisms has been interpreted in terms of the force balance.

From the first set of experiments, we have the following indications with respect to parameter dependence. The number of layers that develops is determined by the thermal Rayleigh number, while it is not very sensitive to the buoyancy ratio. Note that relatively high thermal Rayleigh numbers are necessary to develop multiple layers, which means that a high temperature contrast and/or a large permeability must be present to generate such layers in natural systems. Furthermore, the thickness of a newly formed layer is inversely related to both the buoyancy ratio and porosity, while its dependence on the thermal Rayleigh number is small.

Finally, the large velocities observed in the previous set of experiments indicate that mechanical dispersion may play a role in the transport of chemical elements. The dispersivities of the envisaged geological systems are poorly known, but they seem to depend both on the structure of the rocks and on the scale of the flow domain. To identify the sensitivity of the layer formation to chemical dispersion, we have performed another set of experiments in which the scalar representation of the chemical dispersion is replaced by a more advanced Fickian dispersion model. In this model, which is often used in porous media flow (Bear, 1972), chemical dispersion is related linearly to the chemical gradient by a second order tensor in which the velocity vector and two dispersivities appear.

From the experiments, we observed that mechanical dispersion across the interface tends to reduce the chemical contrast between two convective layers. Since mechanical dispersion increases the entrainment capability of the convective plumes impinging on the interface, the vertical layer scales increases with increasing dispersivities. In case mechanical dispersion dominates the solute transport throughout the domain, the first layer grows to the top without the formation of subsequent layers. Mechanical dis-

persion has been taken into account in the force balance, which determines the limitation of the layer growth.

In the experiments, very sharp internal velocity gradients and also sharp gradients of compositional concentration were observed. In our Fickian formulation of mechanical dispersion, this implies that there are very rapid changes in the dispersion coefficients that could possibly have led to spurious amounts of mixing across the interface due to the diffusive terms.

An alternative for the Fickian form for mechanical dispersion at high concentration gradients was given by Hassanizadeh and Leijnse (1995). These authors argued both theoretically and by means of laboratory experiments that a nonlinear treatment of dispersion explains better the breakthrough of a high concentration gradient during a flushing experiment in a two-dimensional vertical column. Recent experiments show that the amount of dispersion decreases with increasing velocity or concentration gradient (Schotting et al., 1999). In our experiments, this would decrease the amount of dispersion across the interface. Another possibility is that the interface is more of a jump condition in that the upper layer sees very little of the dispersive mixing in the lower layer and does not get as entrained as our formulation might suggest. It would be interesting to resolve the actual dependence of the chemical dispersion behavior in the context of layer formation by physical experiments.

Up to this point, we have described a mechanism by which layered structures can be generated and that can also lead to relatively sudden changes in the layer sequence. In our view, thermochemical convection in porous media offers an interesting explanation for the appearance of layered structures in geological media. Apart from the scenario described here, in which heat is the driving component, the experiments may also represent the situation in which two chemical components produce layering. As an alternative, side wall heating may also lead to the development of horizontally layered structures (see Kranenborg (1997) for a study in purely viscous fluids). For a general discussion of our results with respect to layer formation in magmatic intrusions and the early Earth's mantle, the reader is referred to Schoofs et al. (1998).

Here, we would like to confine the geological discussion to the formation and evolution of layered structures in continental and sub-seafloor hydrothermal systems. These near-surface systems are potentially influenced by the existence of chemically distinct layers (Bischoff and Rosenbauer, 1989; Fournier, 1990; Lowell and Germanovich, 1997). From the results of laboratory experiments in a three-dimensional porous medium, Griffiths (1981) concluded that a brine layer at the base of a hydrothermal system can be maintained. Extrapolating our results, the generation of vertically stacked layers is possible only at sufficiently large thermal Rayleigh numbers and high buoyancy ratios. In other words, the hydrothermal system must be permeable up to considerable depths, while a large initial compositional gradient is present within the liquid. Besides these two constraints, also the porosity and dispersivity of the rocks appear to be critical parameters in determining the stability of the layers.

Once two or more layers have developed within a hydrothermal system, the chemically distinct reservoirs can basically be maintained on a chemically dispersive time scale. During this period, which may last thousands of years, heat (solute) flux through the system is determined by the diffusion (dispersion) across the interfaces. Consequently, the temperature in the upper fluid layer is reduced in comparison to a single-layered system (Griffiths, 1981). Note, however, that interfaces could be destroyed by a dynamical mechanism at an earlier stage in the evolution of the system.

A well-known example of a layered continental hydrothermal system is the Salton Sea Geothermal System, CA, in which a sharp salinity interface has been observed at 0.5–2.5 km depth (Williams, 1997). This interface follows the isotherm of 260°C, rather than any structural or stratigraphic feature, and separates a chemically almost homogeneous liquid with a total amount of dissolved solids exceeding 25 wt.% from the overlying dilute fluids. These observations speak very well for a layered thermochemical convective system, like the one described in this study.

This specific site was recently studied in detail by (Oldenburg and Pruess, 1998). From numerical simulations, these authors concluded that thermochemical convection can explain most of the observations, though the stability of the layers depends critically

on the anisotropic character of the rocks. Layering is favored only when ''horizontal permeability is much larger than the vertical component''. Otherwise, the convection currents penetrate the salinity interface and destroy the layering.

Provided that the force balance (Eq. (19)) is also valid in anisotropic media, this behavior can be explained in a fluid-dynamical context. In an isotropic medium, the density contrast across the salinity interface is not sufficiently strong to keep the layers separated. This leads to a breakup or migration of the interface and subsequent mixing of the two layers. By introducing a large horizontal permeability compared to the vertical component, convection can develop within both layers while the vertical convective forces remain small. As a result, the salinity interface at depth is dynamically sustained.

Besides the layer-formation mechanism described here, finally, the process of supercritical phase separation of seawater has been proposed as another means to produce a saline layer at depth (Bischoff and Rosenbauer, 1989; Lowell and Germanovich, 1997). Especially in hydrothermal systems beneath mid-ocean ridges, the seawater-derived liquids filling the basalts may separate into a dilute vapor phase and a very saline brine after a magmatic event at a few kilometers depth. While the vapor phase vents through the seafloor shortly after the event, the brine phase may accumulate in a continuous brine layer at the base of the system (Lowell and Germanovich, 1997).

In principle, the force balance can be used to determine the stability of the brine layer once the liquid has returned into the single-phase regime. However, realistic (nonlinear) equations of state, heterogeneous and anisotropic permeability, and temperature and chemical dependent viscosity may change significantly the stability of the brine layer, compared to the first-order approximation invoked in this study. The stability of the brine layer in a more realistic setting of the ridge crest is studied explicitly in Schoofs and Hansen (1999).

Acknowledgements

The authors thank Frank Spera, Gualbert Oude Essink and an anonymous referee for constructive comments. The investigations were supported by the Research Council for Earth and Lifesciences (ALW) with financial aid from the Netherlands Organization for Scientific Research (NWO), within the project 750.195.08. The computations were performed on the Cray Y-MP C916 at the Academic Computing Centre (SARA), Amsterdam. Use of these computing facilities was sponsored by the National Computing Facilities Foundation (NCF), within the project SC-492.

References

Aharonov, E., Spiegelman, M., Kelemen, P., 1997. Three-dimensional flow and reaction in porous media: implications for the Earth's mantle and sedimentary basins. J. Geophys. Res. 102, 14821–14833.

Alley, K.M., Parmentier, E.M., 1998. Numerical experiments on thermal convection in a chemically stratified viscous fluid heated from below: implications for a model of lunar evolution. Phys. Earth Planet. Inter. 108, 15–32.

Batchelor, G.K., 1967. An Introduction to Fluid Dynamics. Cambridge University Press, London.

Bear, J., 1972. The Dynamics of Fluids in Porous Media. Dover Publications, New York.

Bischoff, J.L., Rosenbauer, R.J., 1989. Salinity variations in submarine hydrothermal systems by layered double-diffusive convection. J. Geol. 97, 613–623.

Cawthorn, R.G. (Ed.), 1996. Layered intrusions. Developments in Petrology, 15. Elsevier, New York.

Fernando, H.J.S., 1987. The formation of a layered structure when a stable salinity gradient is heated from below. J. Fluid Mech. 182, 525–541.

Fournier, R.O., 1990. Double-diffusive convection in geothermal systems: the Salton Sea, California, geothermal system as a likely candidate. Geothermics 19, 481–496.

Gelhar, L.W., Welty, C., Rehfeldt, K.R., 1992. A critical review of data on field-scale dispersion in aquifers. Water Resour. Res. 28, 1955–1974.

Griffiths, R.W., 1981. Layered double-diffusive convection in porous media. J. Fluid Mech. 102, 221–248.

Hansen, U., Yuen, D.A., 1995. Formation of layered structures in double-diffusive convection as applied to the geosciences. In: Brandt, A., Fernando, H.J.S. (Eds.), Double-Diffusive Convection. Geophys. Monogr. vol. 94.

Hassanizadeh, S.M., Leijnse, A., 1995. A nonlinear theory of high-concentration-gradient dispersion in porous media. Adv. Water Resour. 18, 203–215.

Hundsdorfer, W., Trompert, R.A., 1994. Method of lines and direct discretization: A comparison for linear advection. Appl. Numer. Math. 13, 469–490.

Huppert, H.E., Linden, P.F., 1979. On heating a stable salinity gradient from below. J. Fluid Mech. 95, 431–464.

Kimura, S., Schubert, G., Straus, J.M., 1986. Route to chaos in porous-medium thermal convection. J. Fluid Mech. 166, 305–324.

Kranenborg, E.J., 1997. Double-diffusive convection due to lateral thermal forcing. PhD thesis, IMAU, Utrecht University.

Lowell, R.P., Germanovich, L.N., 1997. Evolution of a brine-saturated layer at the base of a ridge-crest hydrothermal system. J. Geophys. Res. 102, 10245–10255.

McBirney, A.R., Noyes, R.M., 1979. Crystallization and layering of the Skaergaard Intrusion. J. Petrol. 310, 487–554.

Molemaker, M.J., Dijkstra, H.A., 1997. The formation and evolution of a diffusive interface. J. Fluid Mech. 331, 199–229.

Murray, B.T., Chen, C.F., 1989. Double-diffusive convection in a porous medium. J. Fluid Mech. 201, 147–166.

Nield, D.A., Bejan, A., 1992. Convection in Porous Media. Springer, New York.

Oldenburg, C.M., Pruess, K., 1995. Dispersive transport dynamics in a strongly coupled groundwater–brine flow system. Water Resour. Res. 31, 289–302.

Oldenburg, C.M., Pruess, K., 1998. Layered thermohaline convection in hypersaline geothermal systems. Transp. Porous Media 33, 29–63.

Olson, P., Silver, P.G., Carlson, R.W., 1990. The large-scale structure of convection in the Earth's mantle. Nature 334, 209–215.

Phillips, O.M., 1991. Flow and Reactions in Permeable Rocks. Cambridge Univ. Press, New York.

Rosenberg, N.D., Spera, F.J., 1992. Thermohaline convection in a porous medium heated from below. Int. J. Heat Mass Transfer 35, 1261–1273.

Schoofs, S., Hansen, U., 1999. Depletion of a brine layer at the base of ridge-crest hydrothermal systems. Earth Planet. Sci. Lett., submitted for publication.

Schoofs, S., Spera, F.J., Hansen, U., 1999. Chaotic thermohaline convection in low-porosity hydrothermal systems. Earth Planet. Sci. Lett., in press.

Schoofs, S., Trompert, R.A., Hansen, U., 1998. The formation and evolution of layered structures in porous media. J. Geophys. Res. 103, 20843–20858.

Schotting, R.J., Moser, H., Hassanizadeh, S.M., 1999. High-concentration-gradient dispersion in porous media: experiments, analysis and approximations. Adv. Water Resour. 22, 665–680.

Shen, C.Y., Veronis, G., 1991. Scale transition of double-diffusive finger cells. Phys. Fluids A 3, 58–68.

Spera, F.J., Yuen, D.A., Hong, H.-J., 1986. Double-diffusive convection in magma chambers: Single or multiple layers? Geophys. Res. Lett. 13, 153–156.

Stevenson, D.J., 1989. Formation and early evolution of the Earth. In: Peltier, W.R. (Ed.), Mantle Convection. Gordon & Breach, Newark, NJ, pp. 818–873.

Sweby, P.K., 1984. High resolution schemes using flux-limiters for hyperbolic conservation laws. SIAM J. Numer. Anal. 21, 995–1011.

Trompert, R.A., Hansen, U., 1996. The application of a finite volume multigrid method to three-dimensional flow problems in a highly viscous fluid with a variable viscosity. Geophys. Astrophys. Fluid Dyn. 83, 261–291.

Turner, J.S., 1968. The behaviour of a stable salinity gradient heated from below. J. Fluid Mech. 33, 183–200.

Turner, J.S., 1985. Multicomponent convection. Annu. Rev. Fluid Mech. 17, 11–44.

Williams, A.E., 1997. Fluid density distribution in a high temperature, stratified thermohaline system: implications for saline hydrothermal circulation. Earth Planet. Sci. Lett. 146, 121–136.